Atmos. Chem. Phys. Discuss., 10, 20167–20191, 2010
www.atmos-chem-phys-discuss.net/10/20167/2010/
doi:10.5194/acpd-10-20167-2010

Atmospheric Chemistry and Physics Discussions

Ancient versus modern mineral dust transported to high-altitude Alpine glaciers evidences Saharan sources and atmospheric circulation changes

F. Thevenon[1], **M. Chiaradia**[2], **T. Adatte**[3], **C. Hueglin**[4], **and J. Poté**[1]

[1]Institute F.-A. Forel, University of Geneva, Versoix, Switzerland
[2]Department of Mineralogy, University of Geneva, Geneva, Switzerland
[3]Institute of Geology and Palaeontology, University of Lausanne, Lausanne, Switzerland
[4]Empa, Swiss Federal Laboratories for Materials Testing and Research, Dübendorf, Switzerland

Received: 4 June 2010 – Accepted: 11 August 2010 – Published: 25 August 2010

Correspondence to: F. Thevenon (florian.thevenon@yahoo.fr)

Published by Copernicus Publications on behalf of the European Geosciences Union.

Abstract

Mineral dust aerosols collected during the years 2008/2009 at the high-altitude research station Jungfraujoch (46°33′, 7°59′; 3580 m a.s.l.) were compared to windblown mineral dust deposited at the Colle Gnifetti glacier (45°55′ N, 7°52′ E; 4455 m a.s.l.) over the last millennium. Insoluble dust has been characterized in terms of mineralogy, Sr and Nd isotopic ratios, and trace element composition. Results demonstrate that the Saharan origin of the airborne dust did not change significantly throughout the past. Backward trajectories analysis of modern analogs furthermore confirms that major dust sources are situated in the north-central to north-western part of the Saharan desert. By contrast, less radiogenic Sr isotopic compositions are associated with lower abundances of crustal elements during low rates of dust deposition, suggesting intercontinental transport of background dust rather than activation of a secondary source. Saharan dust mobilization and meridional advection of air masses were relatively reduced during the second part of the Little Ice Age (ca. 1690–1870), except within the greatest Saharan dust event deposited around 1780–1790. Higher dust deposition with larger mean grain size and Saharan fingerprint began ca. 20 years after the industrial revolution of 1850, suggesting that increased mineral dust transport over the Alps during the last century was primarily due to drier winters in North Africa and stronger spring/summer North Atlantic southwesterlies, rather than to direct anthropogenic sources. Meanwhile, increasing carbonaceous particle emissions from fossil fuels combustion combined to higher lead enrichment factor during the last century, point to concomitant anthropogenic sources of particulate pollutants reaching high-altitude European glaciers.

1 Introduction

Polar ice core studies document enhanced atmospheric crustal dust transport during glacial/interglacial colder climates, but dust archived in Alpine, Himalayan, and Antarc-

ACPD
10, 20167–20191, 2010

tica ice cores reveal higher continental dust deposition during the 20th-century warming (De Angelis and Gaudichet, 1991; Thompson et al., 2000; McConnell et al., 2007; Thevenon et al., 2009). Moreover, despite the striking increase of mineral dust transported over Europe during the last decades and the associated radiative forcing on climate system (IPCC, 2007), there is a lack of ice-core data about mid-latitude dust characteristics covering the preindustrial period. In order to evaluate European preindustrial atmospheric dust emissions, we have characterized windblown mineral dust archived in an Alpine ice core over the last millennium. In fact, mineralogical and geochemical compositions of the mineral aerosols entrapped in the ice differ according to their geological sources (Grousset and Biscaye, 2005). For instance, strontium (Sr) and neodymium (Nd) isotopic measurements of aeolian dust transported to East Antarctica drilling sites have highlighted efficient transfer of dust from South America during cold Quaternary climates (Delmonte et al., 2010). Similarly, Eastern Asia desert areas were identified as being the main source of dust found in Greenland ice cores from 44 to 14 kyr BP (Svensson et al., 2000). Nevertheless, ice-core records also reveal complex spatial and temporal patterns of variability that require further investigations (Delmonte et al., 2004; Xu et al., 2010; Vallelonga et al., 2010). In order to link aeolian dust sources and associated circulation patterns, we have studied the insoluble dust fraction transported to the Alps during the last millennium. Mineralogical and geochemical fingerprints of the paleodust were then compared to analog aerosols and potential dust source areas.

The Sahara is the world's major source of mineral dust, which subsequently spreads across the Mediterranean and Caribbean seas into northern South America, Central America, North America, and Europe. Grousset and Biscaye (2005) demonstrated by combining Sr and Nd isotopic fingerprinting and air-mass back-trajectory that the geochemical signature of Saharan dust transported to the Alps could be used for paleodust transport studies. Moreover, the Southern Alps act as a barrier to the transport of the southwesterly dust laden winds from the Sahara during the spring and summer seasons. Hence, the Colle Gnifetti glacier saddle, where the oldest glaciological record

ACPD
10, 20167–20191, 2010

over the Alps has been recovered (Jenk et al., 2006), makes a valuable candidate for studying past atmospheric dust sources and associated transport patterns. The objective of this study is 1) to characterize the mineralogy, geochemistry and isotopic composition (Sr and Nd) of aeolian dust windborne over the Alps during the millennium, and 2) to compare the paleodust characteristics to analog aerosols collected at the Jungfraujoch high-alpine research station and with documented Saharan dust sources.

2 Study sites

This study was performed with the samples collected from two sites: i) the Colle Gnifetti glacier saddle (CG, 45°55′ N, 7°52′ E; 4455 m a.s.l.; Fig. 1) is located in the Monte Rosa Massif (the second highest mountain in the Alps), on the southern side of the Alps and on the border between Switzerland and Italy. A previous study has demonstrated that the CG archive (core CG03) allows the reconstruction of changes in the dynamic of the southwesterly dust-laden winds from the Sahara, in relation to variability in large-scale atmospheric circulation patterns (Thevenon et al., 2009). The CG glacier saddle is located at ca. 70 km from ii) the high-alpine research station Jungfraujoch (JFJ, 46°33′ N, 7°59′ E; 3580 m a.s.l.; Fig. 2), which is the highest permanently manned weather station in Europe. This high Alpine site is located on the northern edge of the Swiss Alps, offering a very low background clean continental site for studying changes in the composition of the atmosphere (Nyeki et al., 1997; Overton, 2008). Daily PM_{10} aerosol samples were collected on quartz fiber filters (24 h from midnight to midnight) within the scope of the Swiss National Air Pollution Monitoring Network (NABEL).

ACPD
10, 20167–20191, 2010

3 Analytical methods

3.1 Dust samples and digestion procedure

The CG ice-core dust samples were extracted from cellulose membrane filters mounted on smear slides using Canada balsam, previously analyzed for total aerosols and mineral grain size by image analysis, using the procedure as described in Thevenon et al. (2009). Retrieved filters encompassing insoluble particulate matter were cut in two parts, and placed in 1.5 ml of xylène in an ultrasonic bath for 10 min to dissolve the Canada balsam. Afterward, the original filter was removed, and 5 ml of Milli-Q water was added in each sample. The first half of the ice core sample was filtered on Ag filter for being analyzed by X-ray diffraction, whereas the second part was digested in 1 ml HNO_3 (suprapur, 65%), 2 ml of HF (suprapur, 40%), and 1 ml of $HClO_4$ (suprapur, 70%). Following evaporation at 150 °C, 1 ml of Milli-Q water and 1 ml of HNO_3 (suprapur, 65%) were successively added, and the solution was left to complete evaporation between each step. The resulting solid was finally dissolved in 8 ml of 1% HNO_3 solution for chemical analysis. About 2 ml was used for elemental and REE analysis by ICPMS, while the remainder was further analyzed for isotopic composition by mass spectrometry as described in the Sect. 3.4.

Twelve ambient daily PM_{10} aerosols samples enriched in atmospheric dust and collected between 2008 and 2009 at the high-altitude research station JFJ were selected. The quartz fiber filters (Whatman QMA and Pallflex Tissuquartz) were placed in an ultrasonic bath for 10 min. and prepared following the method described above. Gravimetric filter measurements (PM_{10}) were done by the Swiss National Air Pollution Monitoring Network. When sufficient dust material was present, the mean grain-size was measured with a laser granulometer (Malvern Mastersizer) by laser diffraction, after removing the organic fraction using H_2O_2 treatment.

ACPD
10, 20167–20191, 2010

3.2 Mineralogical analysis by XRD

Bulk dust and clay mineral analyses were performed on Ag filter, with a X'TRA-ARL (Thermoscientific) diffractometer, using a wavelength of λ=1.540562 Å. The peak areas of the clays were identified (2θ) with a WinXRXD profile-fitting program, using a Pearson-7 deconvolution function. Percentages of chlorite (C004 peak at 25.1° 2θ Cukalpha reflection), mica (M001 peak at 8.88°), and kaolinite (K002 peak at 24.9°), were estimated using the following equations:

$$\text{All Clays} = \text{M001} + \text{C002} + \text{K001}, \text{ with}$$

$$\text{K001} = \text{K002}/(\text{K002} + \text{C004}) \times \text{K001} - \text{C002}$$

$$\text{C002} = \text{C004}/(\text{C004} + \text{K002}) \times \text{K001} - \text{C002}$$

3.3 Trace and REE analysis by inductively coupled plasma mass spectrometry (ICP-MS)

The concentration of trace and REE elements (Sc, Ti, Cs, Ba, Hf, Ta, Pb, Th, U, La) in the digested solution was measured using quadrupole-based inductively coupled plasma mass spectrometry (ICP-MS) (HP 4500, Agilent). Total variation coefficients of three replicates sample measurements were smaller than 10%.

3.4 Isotopic analysis by Thermal Ionization Mass Spectrometry (TRITON) analysis

Sr and Nd separation from the solutions prepared as above described was carried out using cascade columns with Sr-spec, TRU-spec and Ln-spec resins following a modified method after Pin et al. (1994). Sr and Nd isotope ratios were measured on a Thermo TRITON mass spectrometer on Faraday cups in static mode using the virtual amplifier mode to eliminate cross-calibration effects on the amplifiers. Sr was loaded on single Re filaments with a Ta oxide solution and measured at a pyrometer-controlled

ACPD
10, 20167–20191, 2010

temperature of 1480 °C in static mode using the virtual amplifier design to cancel out biases in gain calibration among amplifiers. $^{87}Sr/^{86}Sr$ values were internally corrected for fractionation using a $^{88}Sr/^{86}Sr$ value of 8.375209. Raw values were further corrected for external fractionation by a value of +0.03‰, determined by repeated measurements of the SRM987 standard ($^{87}Sr/^{86}Sr$=0.710250). External reproducibility (1 s) of the SRM987 standard is 7 ppm. Nd was loaded on double Re filaments with 1M HNO_3 and measured in static mode with the virtual amplifier design. $^{143}Nd/^{144}Nd$ values were internally corrected for fractionation using a $^{146}Nd/^{144}Nd$ value of 0.7219 and the ^{144}Sm interference on ^{144}Nd was monitored on the mass ^{147}Sm and corrected by using a $^{144}Sm/^{147}Sm$ value of 0.206700. External reproducibility (1σ) of the JNdi-1 standard (Tanaka et al., 2000) is <5 ppm.

4 Results and discussion

Trace element concentrations (Pb, Ti, Ba, Cs, U, and La) were normalized to conservative crustal elements (Sc, Ta, Hf, or Th) which primarily derive from wind-borne soil and rock-dust sources, and expressed in the form of crustal enrichment factors (EFs) after normalization to the mean concentration ratios in the upper continental crust (Wedepohl, 1995). EFs were very low (EF<2) for Ti, Ba, and La, thereby excluding important anthropogenic-induced fluxes of crustal elements (i.e. enhanced dust due to deforestation and agricultural activities). By contrast, Pb, and to a lesser extent Cs and U presented higher EFs (EF>10), suggesting the impact of atmospheric emissions of trace elements from anthropogenic sources (e.g. mining and open pit operations, smelting, nuclear tests).

Variations in crustal element abundances are primarily influenced by total and mineral dust inputs (Fig. 2). Dusty layers exhibit higher trace element enrichments and larger particles (>1.5 µm), whereas the light-coloured layers dust are depleted in heavy and/or incompatible elements and contain smaller particles. Such a distribution pattern suggests the activation of a predominant Saharan-derived dust source (dusty layers)

ACPD
10, 20167–20191, 2010

in conjunction with the background signal recorded during low dust flux (light-coloured layers), rather than distinct contributions of local bedrock (Evans et al., 2004; Moreno et al., 2006). Moreover, the geochemical and mineralogical composition of the dust deposited at CG during the last centuries are quite similar to the composition of the dust collected in 2008 and 2009 at JFJ (Figs. 2, 3, 4 and 5), suggesting an overall similarity in aeolian dust sources through time.

Mineral characterization of CG and JFJ samples reveals strong similarities between modern and ancient dust composition, as well as the ubiquity of three source markers for Saharan dust that are palygorskite, kaolinite/chlorite ratio, and quartz (Table 1) (Glaccum and Prospero, 1980; Avila et al., 1997; Caquineau et al., 2002; Fiol et al., 2005). The clay mineralogy of CG and JFJ is reported on Table 2 and compared on Figure 5, showing rather similar clay composition. The dominant mineral group is mica-muscovite, although occasional contributions of local bedrock might occur. This may be the case, for instance, of the great abundance of mica accompanying the presence of paragonite (a mineral present in the Southern Alps but rare to absent in North Africa) within the end of the greatest Saharan dust about 1790 (Fig. 4). Potassium feldspar and plagioclase were accessorily found in some of the ice-core and analog samples (Fig. 4).

The Sr and Nd isotopic similarity between CG ice core data and the available literature data (Grousset et al., 1998; Grousset and Biscaye, 2005) is remarkable, demonstrating the overall Saharan origin for the paleodust reaching the Alps (Fig. 3). This is particularly evident for the dusty ice-core layers (>100 mm^2 of dust/kg) which contain the larger particles (>1.5 µm), and for the sample covering one century of the Middle Age (1200–1300). However, less radiogenic Sr ratios are observed within the light-coloured layers (<30 mm^2 of dust/kg) or when the impact of the fossil fuel pollution becomes important, as attested by minima of $^{87}Sr/^{86}Sr$ values around 1910, 1935 and 1970, which coincide with maxima anthropogenic Pb deposition at CG (Figs. 2 and 3) and with the greatest lead emissions over Europe (Moor et al., 1996; Weiss et al., 1999). EF_{Pb} reached ca. 375 times background level around 1920, when anthro-

ACPD
10, 20167–20191, 2010

pogenic Pb abruptly increased because of the introduction of leaded petrol (Nriagu et al., 1990). The recent less radiogenic Sr ratios therefore reflect mid-latitude intercontinental dust background properties (i.e., physical weathering processes) and/or anthropogenic contamination (e.g., coal for power and smelting plants, traffic exhausts), rather than an alternative contribution from a deeply chemically weathered source (Lahd Geagea et al., 2008; Moreno et al., 2006). Figure 6 plots the aerosol surface, and the mica and chlorite contents against $^{87}Sr/^{86}Sr$ values to illustrate changes in the Sr radiogenic composition with increasing aerosol deposition and clay characteristics. Higher $^{87}Sr/^{86}Sr$ ratios are found within the dusty layers and also show fair positive correlations with mica content and negative ones with chlorite content, probably due to the geochemical affinity of Rb with K, which is abundant in mica-muscovite but absent in chlorite (Fig. 6). Such features may also explain the fact that the JFJ samples are relatively depleted in radiogenic Sr with respect to CG samples (Fig. 3), since the accumulation time is very low.

Air-mass back-trajectories were calculated for analogs using the Hysplit model (Draxler and Rolph, 2003) in order to identify the source region of the paleodust reaching high-altitude Alpine areas (Collaud Coen et al., 2004). The 315 h back-trajectories reaching JFJ are reported on Fig. 1, illustrating the control of the dust laden winds ($PM_{10} \geq 10\,\mu g/m^3$) by the Westerlies, except for one air-mass trajectory which originated from Northeast (13 May 2009). Generally, windborne Saharan dust was directly transported by the southwesterlies winds across the Mediterranean Sea towards the Alps, although some trajectories presented longer transport pathway (e.g. 25 June 2008). Most of the dust-laden winds had origins over Algeria and to a larger extent the north-central to north-western part of the Saharan desert (i.e. Morocco, Tunisia, Libya, and Mali, Fig. 1). Peculiar air masses trajectories reaching the Alps from the North occurred on the 12 and 14 October 2009, with 315-h back-trajectories transport pathways from North America passing over Greenland and towards the Alps from northerly directions. Although the two corresponding samples are extremely depleted in insoluble material ($PM_{10} < 2\,\mu g/m^3$), their elemental crustal composition does not differ significantly from

ACPD
10, 20167–20191, 2010

other JFJ samples (open squares on Fig. 2). Such results therefore support our assumption of Saharan contribution not only for the strong dust events that were rapidly transported towards the Alps from southerly directions, but also for some of the long-range intercontinental dust transport reaching the Alps from northerly directions. Previous air mass back-trajectories analysis from dust deposition sites in the Alps evidenced Saharan mineral dust but also China loess, transported during several days along a pathway across the eastern North Atlantic and approaching the Alps from northerly direction (Grousset and Biscaye, 2005; Sodemann et al., 2006). CG isotopic data furthermore suggest that intercontinental Saharan dust sources might contaminate glacial ice at summit Greenland and that Asian dust (e.g., Gobi desert) might reach the Alpine summits after long-range intercontinental transport within northwesterly winds (Burton et al., 2006; Svensson et al., 2000) (Fig. 3).

Long-term variations of Saharan dust transport to Alpine glaciers reflect atmospheric circulation changes over the Northern Hemisphere (Kang et al., 2003). Higher dust deposition at CG as evidenced during the first part of the Little Ice Age (LIA) (i.e., before ca. 1690), within the greatest event of the millennium (ca. 1780–1790), and after 1870, therefore strongly suggests winter drought conditions over North Africa and/or stronger spring/summer pressure gradient over the North Atlantic (Chiapello and Moulin, 2002). By contrast, low dust deposition during the latter part of LIA (from ca. 1690 to 1870), reflects weakened pressure gradient across the North Atlantic region and increased rainfall in northern Africa (Glueck and Stockton, 2001; Thevenon et al., 2009). Weaker summer southwesterlies trade winds inferred from CG dust record during the latter part of the LIA, are consistent with the synchronous decline of the meridional overturning circulation (MOC) and increased negative states of the North Atlantic Oscillation (NAO) (Shindell et al., 2001; Lund et al., 2006).

Post-1850 increase in carbonaceous residues of combustion, or black carbon (BC), and in trace elements content, likely highlighted additional human impact on recent insoluble pollutant emissions (Fig. 2). The isotopic composition of the soot carbon ($\delta^{13}C_{BC}$) reflects dominant C_3 ($\delta^{13}C$=-27‰) woody pyrogenic emissions or fossil coal

ACPD
10, 20167–20191, 2010

burning, while the decreasing trend observed in the $\delta^{13}C_{BC}$ during the last century likely reflects increasing relative contribution from fossil fuel emissions (^{13}C Suess effect; Thevenon et al., 2009) (Fig. 2). Polycyclic Aromatic Hydrocarbons (PAHs) analysis from CG core also reveals exponentially increasing PAHs emissions from 1900, reaching maxima concentration levels in 1920 and 1940–1950 (Gabrieli, 2008). The present record, which ends with the 1977 Saharan dust event, therefore agrees with a strong decrease of anthropogenic pollutant emissions in the 1960s–1970s (Pb and U on Fig. 2), thanks to more efficient emissions control. Nonetheless, PAHs data furthermore show a renewed increase of anthropogenic pollutant emissions from 1975 to 2003 (Gabrieli, 2008). Additional data with a large spatial representation from shallow snow cores would therefore be necessary to assess seasonal changes of natural and anthropogenic trace elements deposition, with respect to sources and atmospheric pathways.

5 Conclusions

Mineral dust characterization reveals a dominant Saharan-derived source for the dust transported by southwesterly winds, and a subordinate background component linked to northwesterly winds, which becomes evident during periods of low dust deposition. Lower dust inputs in the ice core are depleted in crustal elements and in radiogenic Sr, supporting the occurrence of a background dust source and/or recent pollution contamination, rather than the activation of a secondary dust source. Mineralogical composition and Sr and Nd isotopic composition furthermore suggest that the Saharan intercontinental dust source is not only transported to the top of the Alps but also occasionally reaches Summit Greenland, and that Asian dust contaminates Alpine ice. We highlight that continuous geochemical and mineralogical records of paleodust provide independent and complementary approaches to reconstruct dust sources and atmospheric circulation changes. Trace/crustal elements abundance (e.g. Ti, Ba, La), mineral composition (e.g. clay mineralogy), and isotopic analysis ($^{87}Sr/^{86}Sr$) shows

ACPD
10, 20167–20191, 2010

that North Africa was the most important supplier of dust to mid-latitudes in the Northern Hemisphere. Long-term and continuous records of airborne dust characteristics in climatic archives provide new perspectives on our understanding of seasonal atmospheric circulation changes and large-scale atmospheric teleconnection patterns (e.g. NAO, MOC).

Acknowledgements. We thank M. Collaud Coen and Denis Fontignie for instructive discussions and Michèle Senn for technical support in the sample preparation. We are grateful to the Colle Gnifetti consortium for providing the ice core samples. The present research work was financially supported by a grant from the Swiss National Science Foundation (SNSF Ambizione fellowship).

References

Avila, A., Queralt-Mitjans, I., and Alarcón, M.: Mineralogical composition of African dust delivered by red rains over northeastern Spain, J. Geophys. Res., 102(D18), 21977–21996, 1997.

Burton, G. R., Rosman, K. J. R., Van de Velde, K. P., and Boutron, C. F.. A two century record of strontium isotopes from an ice core drilled at Mt Blanc, France. Earth Planet. Sci. Lett., 248, 202–211, 2006.

Caquineau, S., Gaudichet, A., Gomes, L., and Legrand, M.. Mineralogy of Saharan dust transported over northwestern tropical Atlantic Ocean in relation to source regions, J. Geophys. Res., 107(D15), 4251, doi:10.1029/2000JD000247, 2002.

Chiapello, I. and Moulin, C.: TOMS and METEOSAT satellite records of the variability of Saharan dust transport over the Atlantic during the last two decades (1979–1997), Geophys. Res. Lett., 29, 17–20, 2002.

Collaud Coen, M., Weingartner, E., Schaub, D., Hueglin, C., Corrigan, C., Henning, S., Schwikowski, M., and Baltensperger, U.: Saharan dust events at the Jungfraujoch: detection by wavelength dependence of the single scattering albedo and first climatology analysis, Atmos. Chem. Phys., 4, 2465–2480, doi:10.5194/acp-4-2465-2004, 2004.

De Angelis, M. and Gaudichet, A.. Saharan dust deposition over Mont Blanc (French Alps) during the last 30 years, Tellus, 43B, 61–75, 1991.

ACPD

10, 20167–20191, 2010

Delmonte, B., Andersson, P. S., Schoberg, H., Hansson, M., Petit, J. R., Delmas, R., Gaiero, D. M., Maggi, V., and Frezzotti, M.: Geographic provenance of Aeolian dust in East Antarctica during Pleistocene glaciations: preliminary results from Talos Dome and comparison with East Antarctic and new Andean ice core data, Quaternary Sci. Rev., 29, 256–264, 2010.

Delmonte, B., Petit, J.-R., Andersen, K., Basile-Doelsch, I., Maggi, V., and Lipenkov, V.: Dust size evidence for opposite regional atmospheric circulation changes over east Antarctica during the last climatic transition, Clim. Dynam., 23, 427–438, 2004.

Draxler, R. R. and Rolph, G. D.: HYSPLIT (HYbrid Single-Particle Lagrangian Integrated Trajectory) Model access via NOAA ARL READY Website (http://www.arl.noaa.gov/ready/hysplit4.html), NOAA Air Resources Laboratory, Silver Spring, MD, 2003.

Evans, R. D., Jefferson, I. F., Kumar, R., O'Hara-Dhand, K., and Smalley, I. J.: The nature and early history of airborne dust from North Africa; in particular the Lake Chad basin, J. African Earth Sci., 39, 81–87, 2004.

Fiol, L. A., Fornos, J. J., Gelabert, B., and Guijarro, J. A.: Dust rains in Mallorca (western Mediterranean): their occurrence and role in some recent geological processes, Catena, 63(1), 64–84, 2005.

Gabrieli, J.: Trace elements and Polycyclic Aromatic Hydrocarbons (PAHs) in snow and ice sampled at Colle Gnifetti, Monte Rosa (4450 m), during the last 10,000 years: environmental and climatic implications, PhD 00407177, Université Joseph-Fourier – Grenoble I, 2008.

Gerstenberger, H. and Haase, G.: A highly effective emitter substance for mass spectrometric Pb isotope ratio determinations, Chem. Geol., 136, 309–312, 1997.

Glaccum, R. and Prospero, J. M.: Sahara aerosols over the tropical North-Atlantic Mineralogy, Mar. Geol., 37, 295–321, 1980.

Glueck, M. F. and Stockton, C. W.: Reconstruction of the North Atlantic Oscillation, 1429–1983, Int. J. Climatol., 21, 1453–1465, 2001.

Grousset, F. E. and Biscaye, P. E.: Tracing dust sources and transport patterns using Sr, Nd and Pb isotopes, Chem. Geol., 222, 149–167, 2005.

Grousset, F. E., Parra, M., Bory, A., Martinez, P., Bertrand, P., Shimmield, G., and Ellam, R. M.: Saharan wind regimes traced by the Sr–Nd isotopic composition of subtropical Atlantic sediments: Last Glacial Maximum vs today, Quaternary Sci. Rev., 17, 395–409, 1998.

IPCC: Contribution of Working Group I to the Fourth Assessment Report of the Intergovernmental Panel on Climate Change Fourth Assessment Report, Climate Change 2007: The Physical Science Basis, Summary For Policymakers, available at: www.ipcc.ch, 2007.

ACPD
10, 20167–20191, 2010

Jacobsen, S. B. and Wasserburg, G. J.: Sm-Nd isotopic evolution of chondrites, Earth Planet. Sci. Lett., 50, 139–155, 1980.
Jenk, T. M., Szidat, S., Schwikowski, M., Gäggeler, H. W., Brütsch, S., Wacker, L., Synal, H.-A., and Saurer, M.: Radiocarbon analysis in an Alpine ice core: record of anthropogenic and biogenic contributions to carbonaceous aerosols in the past (1650–1940), Atmos. Chem. Phys., 6, 5381–5390, doi:10.5194/acp-6-5381-2006, 2006.
Kang, C., Mayewski, P. A., Yan, Y., Qin, D., Yao, T., and Ren, J.: Dust records from three ice cores: relationships to spring atmospheric circulation over the Northern Hemisphere, Atmos. Environ., 37(34), 4823–4835, 2003.
Lahd Geagea, M., Stille, P., Gauthier-Lafaye, F., and Millet, M.: Tracing of industrial aerosol sources in an urban environment using Pb, Sr and Nd isotopes, Environ. Sci. Technol., 42, 692–698, 2008.
Lund, D. C., Lynch-Stieglitz, J., and Curry, W. B.: Gulf Stream density structure and transport during the past millennium, Nature, 444, 601–604, 2006.
McConnell, J. R., Aristarain, A. J., Banta, J. R., Edwards, R. P., and Simoes, J. C.: 20th Century doubling in dust archived in an Antarctic Peninsula ice core parallels climate change and desertification in South America, P. Natl. Acad. Sci., 104(14), 5743–5748, 2007.
Moor, H. C., Schaller, T., and Sturm, M.: Recent changes in stable lead isotope ratios in sediments of Lake Zug, Switzerland, Environ. Sci. Technol., 30, 2928–2933, 1996.
Moreno, T., Querol, X., Castillo, S., Alastuey, A., Cuevas, E., Herrmann, L., Mounkaila, M., Elvira, J., and Gibbons, W.: Geochemical variations in aeolian mineral particles from the Sahara-Sahel dust corridor, Chemosphere, 65, 261–270, 2006.
Nriagu, J.: Global metal pollution: poisoning the biosphere, Environment, 32, 28–32, 1990.
Nyeki, S., Li, F., Rosser, D., Colbeck, I., and Baltensperger, U.: The background aerosol size distribution at a high-alpine site: an analysis of the seasonal cycle, J. Aerosol Sci., 28(1), 211–212, 1997.
Overton, A. K.: Jungfraujoch high altitude research station, Weather, 63(3), 76–79, 2008.
Pin, C., Briot, D., Bassin, C., and Poitrasson, F.: Concomitant separation of strontium and samarium-neodymium for isotopic analysis in silicate samples, based on specific extraction chromatography, Anal. Chim. Acta, 298(2), 209–217, 1994.
Shindell, D. T., Schmidt, G. A., Mann, M. E., Rind, D., and Waple, A.: Solar forcing of regional climate change during the Maunder Minimum, Science, 294, 2149–2152. doi:10.1126/science.1064363, 2001.

ACPD
10, 20167–20191, 2010

Sodemann, H., Palmer, A. S., Schwierz, C., Schwikowski, M., and Wernli, H.: The transport history of two Saharan dust events archived in an Alpine ice core, Atmos. Chem. Phys., 6, 667–688, doi:10.5194/acp-6-667-2006, 2006.

Svensson, A., Biscaye, P. E., and Grousset, F. E.: Characterization of late glacial continental dust in the Greenland Ice Core Project ice core, J. Geophys. Res., 105(D4), 4637–4656, 2000.

Tanaka, T., Togashi, S., Kamioka, H., Amakawa, H., Kagami, H., Hamamoto, T., Yuhara, M., Orihashi, Y., Yoneda, S., Shimizu, H., Kunimaru, T., Takahashi, K., Yanagi, T., Nakano, T., Fujimaki, H., Shinjo, R., Asahara, Y., Tanimizu M., and Dragusanu, C.: JNdi-1: a neodymium isotopic reference in consistency with LaJolla neodymium, Chem. Geol., 168, 279–281, 2000.

Thevenon, F., Anselmetti, F. S., Bernasconi, S. M., and Schwikowski, M.: Mineral dust and elemental black carbon records from an Alpine ice core (Colle Gnifetti glacier) over the last millennium, J. Geophys. Res., 114, D17102, doi:10.1029/2008JD011490, 2009.

Thompson, L. G., Yao, T., Mosley-Thompson, E., Davis, M. E., Henderson, K. A., and Lin, P.-N.: A high-resolution millennial record of the South Asian monsoon from Himalayan ice cores, Science, 289, 1916–1919, doi:10.1126/science.289.5486.1916, 2000.

Todt, W., Cliff, R. A., Hanser, A., and Hofmann, A. W.: Evaluation of a ^{202}Pb–^{205}Pb double spike for high-precision lead isotope analysis, in: Earth Processes: Reading the Isotopic Code, edited by: Basu, A. and Hart, S. R., Am. Geophys. Union Geophysical Monograph, 95, 429–437, 1996.

Vallelonga, P., Gabrielli, P., Balliana, I., Wegner, A., Delmonte, B., Turetta, C., Vanhaecke, F., Rosman, K. J. R., Hong, S., Boutron, C. F., Cescon, P., and Barbante, C.: Lead isotopic compositions in the EPICA Dome C ice core and Southern Hemisphere Potential Source Areas, Quaternary Sci. Rev., 29, 247–255, 2010.

Wedepohl, K. H.: The composition of the continental crust, Geochim. Cosmochim. Acta, 59, 1217–1232, 1995.

Weiss D., Shotyk, W., and Kempf, O.: Archives of atmospheric lead pollution, Naturwissenschaften, 86, 262–275, 1999.

Xu, J., Hou, S., Qin, D., Kaspari, S., Mayewski, P. A., Petit, J. R., Delmonte, B., Kang, S., Ren, J., Chappellaz, J., and Hong, S.: A 108.83-m ice-core record of atmospheric dust deposition at Mt. Qomolangma (Everest), Central Himalaya, Quaternary Res., 73, 33–38, 2010.

ACPD
10, 20167–20191, 2010

Table 1. Sample name, age of sample, $^{87}Sr/^{86}Sr$ and $^{143}Nd/^{144}Nd$ isotopic compositions with 2σ (2 standard errors of the mean), and Nd isotopic ratios expressed as epilon units.

Sample name	Age of sample	$^{87}Sr/^{86}Sr$ FC*	2σ Sr $\times10^{-6}$	$^{143}Nd/^{144}Nd$ FC**	2σ Nd $\times10^{-6}$	$\varepsilon_{Nd}(0)$***
33	1975	0.719775	2	0.511998	21	−12.5
34	1973	0.713703	14	0.512335	199	−5.9
36	1971	0.709416	12	0.511623	262	−19.8
37	1969	0.717248	13	0.512081	68	−10.9
38	1968	0.714732	15	0.511865	203	−15.1
44	1956	0.716986	5	0.511993	19	−12.6
48	1951	0.712315	25	0.511908	74	−14.2
49	1948	0.712284	26	0.512069	197	−11.1
53	1937	0.718733	14	0.511986	25	−12.7
55	1934	0.712936	51	0.511722	139	−17.9
58	1924	0.720629	3	0.511957	51	−13.3
60	1919	0.716637	20	0.512135	103	−9.8
61	1913	0.709494	42	–	–	–
64	1905	0.723513	7	0.511929	18	−13.8
66	1898	0.713982	20	0.512110	40	−10.3
68	1889	0.715272	12	0.511999	53	−12.5
70	1880	0.719117	2	0.512011	11	−12.2
72	1873	0.714151	21	0.511907	108	−14.3
73	1860	0.711404	18	0.512005	55	−12.4
77	1846	0.713235	9	0.512090	17	−10.7
81	1811	0.711326	10	0.511911	44	−14.2
84	1796	0.716228	15	0.511956	25	−13.3
85	1790	0.726190	4	0.511967	8	−13.1
86	1786	0.711900	15	0.511968	72	−13.1
90	1769	0.712842	6	0.512382	28	−5.0
92	1743	0.712277	20	–	–	–

ACPD
10, 20167–20191, 2010

Table 1. Continued.

Sample name	Age of sample	$^{87}Sr/^{86}Sr$ FC*	2σ Sr $\times 10^{-6}$	$^{143}Nd/^{144}Nd$ FC**	2σ Nd $\times 10^{-6}$	$\varepsilon_{Nd}(0)$***
93	1726	0.710148	23	0.511809	118	−16.2
94	1714	0.711321	16	0.511950	43	−13.4
95	1700	0.712921	63	0.511975	53	−12.9
96	1686	0.716865	34	0.512066	46	−11.2
97	1672	0.715511	10	0.511990	31	−12.6
98	1655	0.709537	15	0.512169	99	−9.1
99	1637	0.712651	20	0.511995	66	−12.6
100	1619	0.712811	30	0.511856	62	−15.2
101	1600	0.715854	11	0.511964	57	−13.2
102	1580	0.712714	37	0.512184	245	−8.9
104	1544	0.714821	169	0.511771	43	−16.9
105	1511	0.715864	5	0.511949	35	−13.4
110+111	1200-1300	0.717380	1	0.512051	14	−11.5
A	25.06.2008	0.710311	2	0.511958	22	−13.3
B	07.08.2008	0.713474	24	0.512088	75	−10.7
C	09.09.2008	0.710946	5	0.512012	10	−12.2
D	10.09.2008	0.710859	1	0.512042	4	−11.6
E	12.10.2009	0.710600	5	0.512063	19	−11.2
F	14.10.2009	0.710728	5	0.512008	9	−12.3
G	13.05.2009	0.710740	2	0.512088	27	−10.7
H	24.05.2009	0.710430	1	0.512064	33	−11.2
I	28.05.2008	0.709737	8	0.512040	8	−11.7
J	01.06.2008	0.710570	4	0.512057	21	−11.3
K	11.09.2008	0.711140	3	0.512018	6	−12.1
L	13.10.2008	0.712981	5	0.512036	20	−11.7

* All values corrected for internal mass fractionation by normalizing to $^{86}Sr/^{88}Sr$=0.1194 and for external fractionation by normalizing the measured SRM987 values to a SRM987 nominal value of 0.710248.

** All values corrected for internal mass fractionation by normalizing to $^{146}Nd/^{144}Nd$=0.7219 and for external fractionation by normalizing the measured Jndi-1 values to a Jndi-1 value of 0.512115 (Tanaka et al., 2000).

*** calculated for a present-day CHUR value of $^{143}Nd/^{144}Nd$=0.512638 (Jacobsen and Wasserburg, 1980).

ACPD
10, 20167–20191, 2010

Table 2. X-ray mineral compositions for the Colle Gnifetti (CG) ice core samples (upper part), and for the analog samples collected at the Jungfraujoch (JFJ) (lower part). K/C for kaolinite/Chlorite ratio. The symbol plus reflects the abundance of minerals.

Age of sample	%Micas	%Kaolinite	%Chlorite	K/C	Palygorskite	%Paragonite	Quartz
1976	41	38	12	3.22	++	+	+++
1971	46	16	21	0.73	–	+	–
1969	44	19	10	1.86	+	+	+
1967	50	11	11	1.00	+	+	–
1956	41	25	17	1.49	++	+	++
1938	45	18	12	1.50	++	+	+
1924	55	25	20	1.21	+	–	+++
1920	57	23	20	1.13	++	–	++
1880	57	19	11	1.76	++	+	++
1789	83	4	7	0.58	+++	+	+++
1786	46	23	13	1.80	+++	+	++
1580	62	16	22	0.73	+	–	+
01.06.2008	47	30	23	1.31	++	–	+++
25.06.2008	34	22	45	0.48	+	–	+++
07.08.2008	39	28	33	0.85	+	–	+++
09.09.2008	52	23	25	0.93	++	–	+++
10.09.2008	51	31	18	1.67	++	+	++
11.09.2008	45	28	28	1	+	–	–
12.10.2009	44	30	25	1.19	++	–	+++

ACPD
10, 20167–20191, 2010

Table 3. The backward trajectory arrival date and source countries of the Sahara dust events sampled at the Jungfraujoch (JFJ), PM_{10} values, and mean grain-size.

Backward trajectory arrival date and origin (Fig. 1)			PM_{10} ($\mu g/m^3$)	Mean (μm)
28.05.2008	20 h	Libya, Tunisia	26.2	–
01.06.2008	17 h	Morocco, Algeria, Tunisia	12	4.0
25.06.2008	23 h	Libya, Tunisia, Algeria	45.1	3.9
07.08.2008	3 h	Morocco	9.8	4.0
09.09.2008	18 h	Algeria	27.9	3.9
10.09.2008	18 h	Libya, Tunisia, Algeria	58.7	3.4
11.09.2008	15 h	Algeria	46.9	–
13.10.2008	21 h	Algeria, Mali	38.7	–
13.05.2009	20 h	Libya, Algeria	19	3.8
24.05.2009	23 h	Morocco, Algeria	22.2	4.3
12.10.2009	23 h	West via Greenland	1.1	–
14.10.2009	12 h	West via Greenland	1.3	–

ACPD
10, 20167–20191, 2010

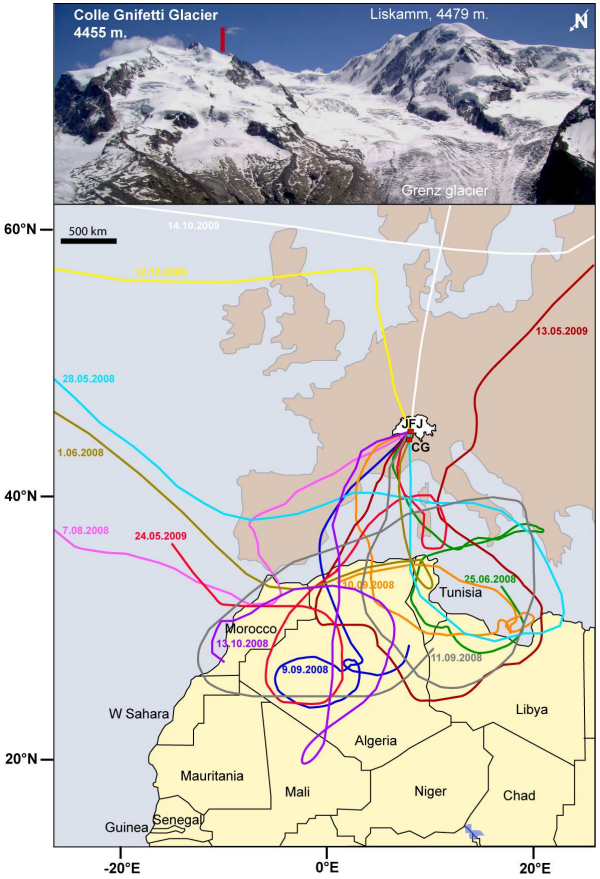

Fig. 1. (top) Panorama from the south of the Monte Rosa Massif showing the location of the ice core site (Colle Gnifetti glacier, CG). (bottom) Geographical map showing the 315-h backward trajectories arriving at Jungfraujoch (JFJ), reconstructed using the NOAA Hysplit model (http://ready.arl.noaa.gov/HYSPLIT.php).

ACPD
10, 20167–20191, 2010

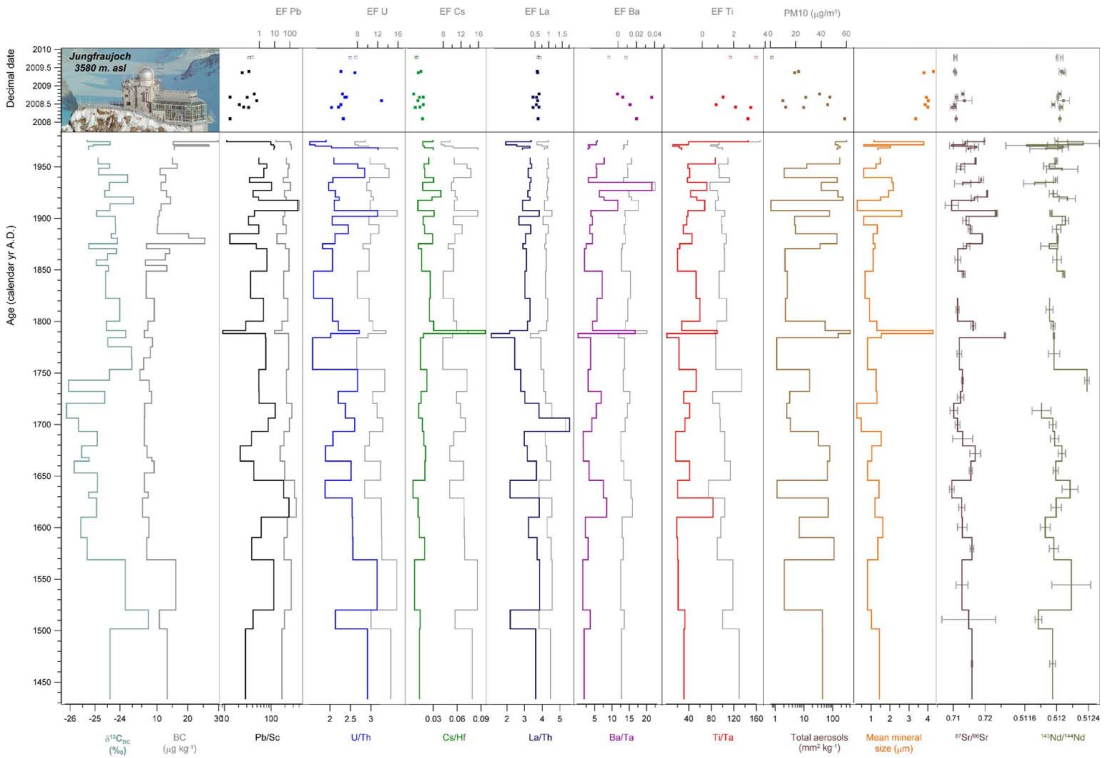

Fig. 2. (left insert) Aerial view of the Jungfraujoch (JFJ) research station. The record of black carbon (BC) concentration and the associated $\delta^{13}C_{BC}$ composition (Thevenon et al., 2009), as a function of age (calendar year AD). Trace element concentrations (Pb, Ti, Ba, Cs, U, and La) normalized to conservative crustal elements (Sc, Ta, Hf, or Th), and crustal enrichment factors (EFs) after normalization to the mean concentration ratios in the upper continental crust (Wedepohl, 1995). The total aerosols surface and the mean diameter of the mineral fraction (Thevenon et al., 2009) compared to Sr and Nd isotopic ratios. The analyses of analog samples collected during the years 2008/2009 at the JFJ are reported in the upper part. $^{87}Sr/^{86}Sr$ error bars (2 standard errors of the mean) have been multiplied by 5 for CG samples and by 10 for JFJ samples.

ACPD
10, 20167–20191, 2010

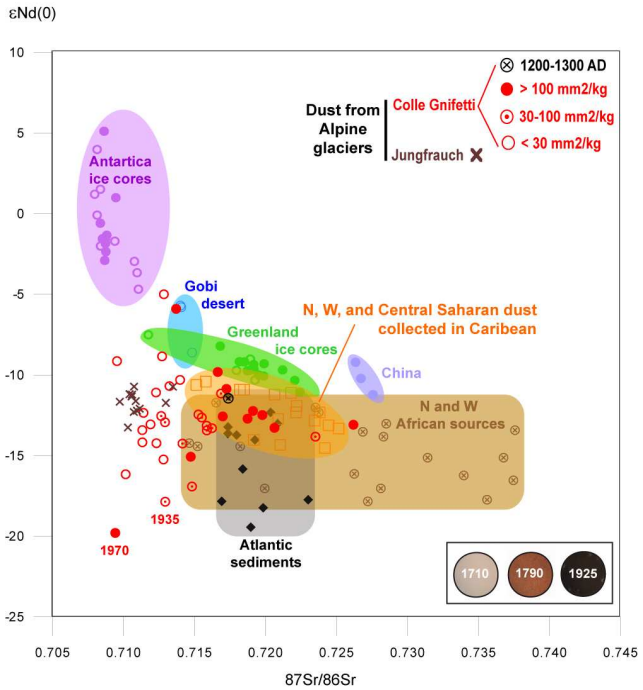

Fig. 3. Sr and Nd isotopic data from Jungfraujoch samples (JFJ, crosses), and from Colle Gnifetti ice core (CG, filled circles) as a function of the total aerosol surface, compared to: glacial dust values from East Antartica ice cores (filled circles: Dome C, empty circles: Vostok), Gobi desert, China loess, Greenland ice core (empty circles: GISP2), Greenland ice core (filled circles, GRIP), <30 µm fraction of Atlantic sediments (filled diamond), North African and central-Sahara/Sahel derived aerosols recovered over the island of La Martinique (Caribbean, empty squares), and north African sand deposits (closed circles). The digital images of three filters, respectively depleted in insoluble minerals (ca. 1710), enriched in Saharan dust (ca. 1790), and enriched in fossil fuel combustion products (ca. 1925). Data sources: Biscaye et al. (1997); Grousset et al. (1998); Svensson et al. (2000); Delmonte et al. (2004); Grousset et al. (2005).

ACPD
10, 20167–20191, 2010

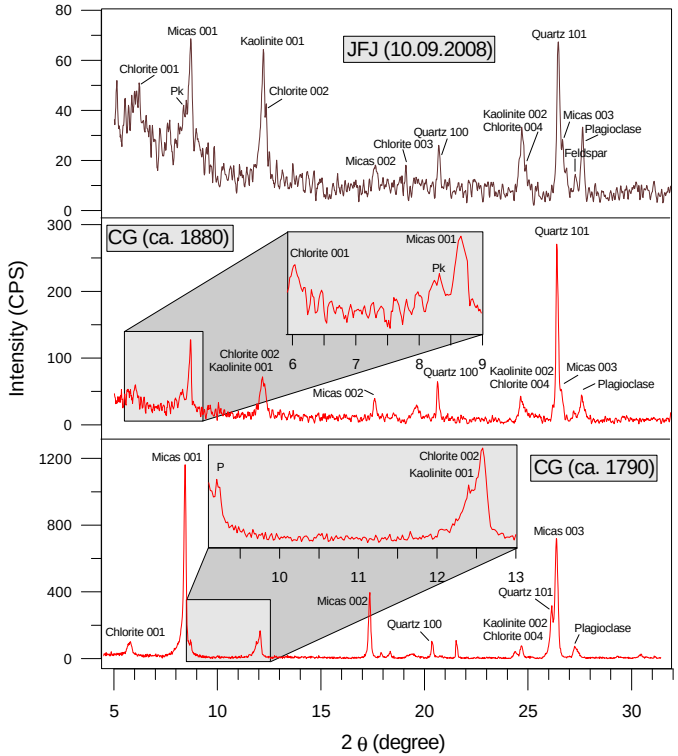

Fig. 4. X-ray diffraction (XRD) spectra of a Jungfraujoch sample (JFJ, upper spectrum), and from two Colle Gnifetti ice core (CG) samples enriched in Saharan dust. The minerals and the Miller indices associated with the major peaks are indicated. P: paragonite, and Pk: palygorskite.

ACPD
10, 20167–20191, 2010

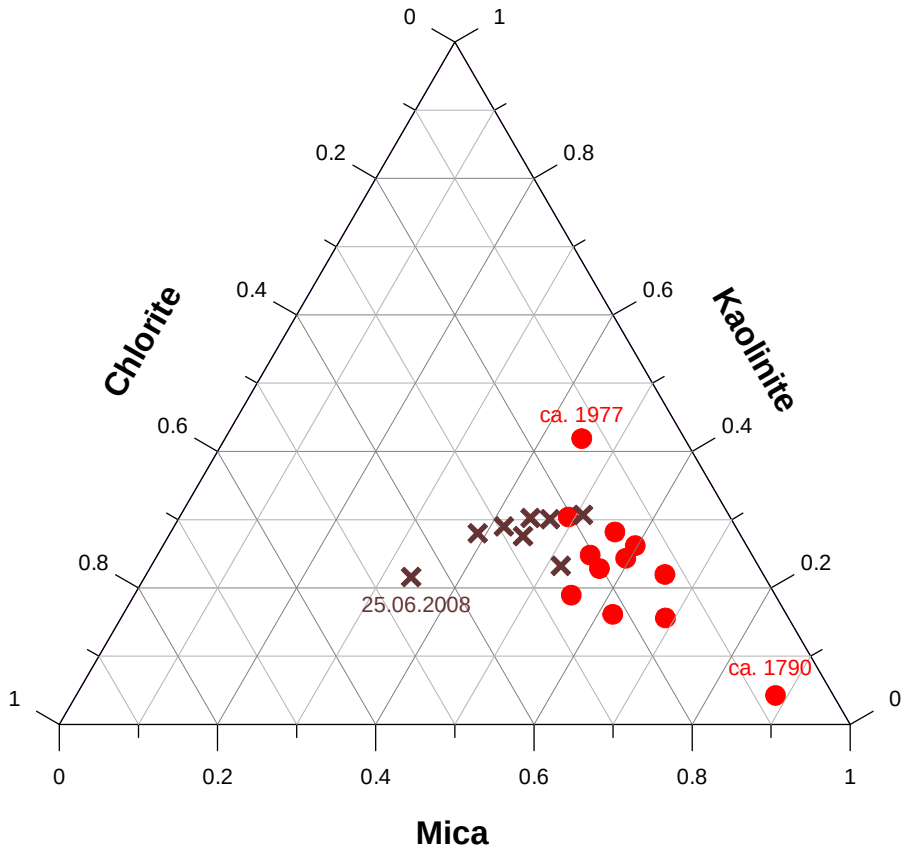

Fig. 5. Kaolinite-Mica-Chlorite triangular diagram illustrating the clay mineralogy of Colle Gnifetti ice core (CG, circles) and Jungfraujoch samples (JFJ, crosses).

ACPD
10, 20167–20191, 2010

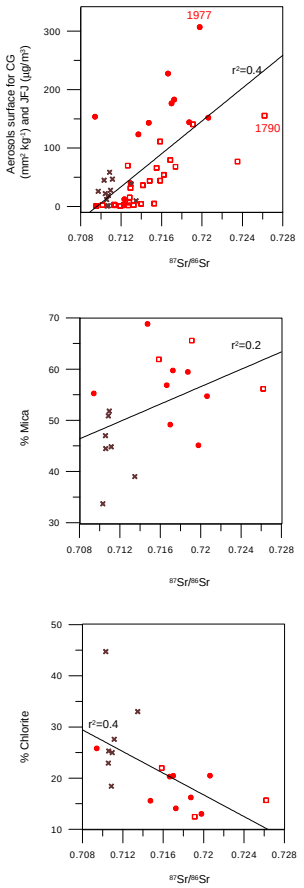

Fig. 6. $^{87}Sr/^{86}Sr$ values as a function of the aerosol surface, the mica and chlorite contents, for the Colle Gnifetti ice core (CG, circles) and Jungfraujoch samples (JFJ, crosses). Pre-1910 CG samples are represented by empty squares, whereas post-1910 samples are represented by filled circles.

ACPD
10, 20167–20191, 2010